Molecularly imprinted cyclodextrin nanosponges for the controlled delivery of L-DOPA: perspectives for the treatment of Parkinson's disease

Molecularly imprinted cyclodextrin nanosponges for the controlled delivery of L-DOPA: perspectives for the treatment of Parkinson's disease

Francesco Trotta[1]*, Fabrizio Caldera[1], Roberta Cavalli[2], Marco Soster[2], Chiara Riedo[1], Miriam Biasizzo[1], Gloria Uccello Barretta[3], Federica Balzano[3], Valentina Brunella[1]

1. Dipartimento di Chimica – University of Torino – Via Pietro Giuria 7, 10125 Torino – Italy

2. Dipartimento di Scienza e Tecnologia del Farmaco - University of Torino – Via Pietro Giuria 9, 10125 Torino – Italy

3. Dipartimento di Chimica e Chimica industriale – University of Pisa – Via Giuseppe Moruzzi 3, 56124 Pisa – Italy

***** Author for correspondence e-mail francesco.trotta@unito.it Phone number +39 011 6707550 Fax +39 011 6707855

Keywords. Cyclodextrins; in vitro release studies; inclusion compounds; L-DOPA; molecularly Imprinted Polymers; Nanosponges

ABSTRACT

Background L-DOPA is an amino acid precursor to the neurotransmitter dopamine that is extensively used as a prodrug for the treatment of Parkinson's disease. However, L-DOPA is an unstable compound: when exposed to light or added to aqueous solutions, it may degrade, compromising its therapeutic properties.

Research design and methods In this work, a new type of drug-loaded cyclodextrin-based nanosponge, obtained using molecular imprinting, is described for the prolonged and controlled release of L-DOPA. The molecularly imprinted nanosponges (MIP-NSs) were synthesized by cross-linking β-cyclodextrin with 1,1'-carbonyldiimidazole in DMF in the presence of L-DOPA as a template molecule. TGA, DSC and FTIR analyses were performed to characterize the interactions between L-DOPA and the two nanosponge structures. Quantitative NMR spectroscopy was used to determine the amount and the affinity of L-DOPA entrapped in the nanosponges. The *in vitro* L-DOPA release kinetics from the NSs were quantitatively determined by HPLC analysis.

Results The MIP-NSs show a slower and more prolonged release profile than the non-imprinted nanosponges. No degradation of the L-DOPA hosted in the MIP-NSs was observed after long-term storage at room temperature.

Conclusions The MIP-NSs are a promising alternative for the storage and controlled delivery of L-DOPA.

INTRODUCTION

L-DOPA [(S)-2-amino-3-(3,4-dihydroxyphenyl) propanoic acid] is a non-proteinogenic amino acid, precursor to the neurotransmitter dopamine [1]. The lack of dopamine is at the base of Parkinson's disease (PD), which afflicts approximately 0.3 % of the entire population, causing symptoms such as tremors, rigidity, bradykinesia and akinesia [2]. The administration of dopamine is completely ineffective as a treatment for PD because dopamine is not able to cross the blood-brain barrier, while L-DOPA can reach the central nervous system and be converted, via decarboxylation [3,4] by the neuronal amino acid decarboxylase, into dopamine. More exactly, L-DOPA acts as a prodrug that is absorbed in the small intestine and carried to the brain by the blood stream.

L-DOPA is currently the most widely used drug for the treatment of PD. However, it is an unstable compound; when exposed to light or added to aqueous solution (especially basic solution), it may degrade, compromising its therapeutic properties. Approximately 99 % of orally administered L-DOPA is degraded through peripheral decarboxylation and oxidation [5,6]. The remaining 1 % can reaches the brain unchanged. To reduce the peripheral conversion of this drug into dopamine, carbidopa and benserazide are usually added to the drug formulation as inhibitors of the decarboxylase activity [1-6].

Additionally, it is not possible to reach and maintain a constant L-DOPA plasma concentration via oral administration of conventional immediate-release systems because the concentration fluctuates widely with time [7]. Consequently, it is difficult to control the symptoms of PD and allow patients to achieve a satisfying quality of life.

Many other administration routes have been explored to stabilize the L-DOPA concentration in the blood. Good results have been obtained with intravenous [8] and intra-duodenal infusions of L-DOPA [9]; however, these treatments are time-consuming and continuous medical assistance is required.

The implantation of long-term L-DOPA releasing systems has also been investigated [10]. However, despite the positive results, implantation remains an invasive and problematic technique.

Transdermal delivery systems represent an interesting and easy alternative that could provide long-term sustained release of the drug. Since L-DOPA is a polar compound, it cannot easily cross the lipid barrier of the skin; therefore, organic solvents have been employed to increase the cutaneous permeability of the drug. Studies conducted on rats have been successful, but the effects of these dermal treatments on humans are still unknown [11]. Encouraging results have also been achieved using gastroretentive delivery systems. Since L-DOPA is mostly absorbed in the first part of the small intestine (duodenum), gastroretentive delivery systems have been developed with the aim of prolonging the release of the drug in the area of maximal absorbance. Studies have not yet been performed in humans [12]. Odak *et al.* used highly soluble hydroxypropylated β-cyclodextrin to form

stable complexes with L-DOPA. The stability, aqueous solubility and consequently the bioavailability of the drug were increased [13]. The use of microscopic and nanoscopic carriers as drug delivery systems is one of the most promising approaches to both achieving a constant L-DOPA plasma concentration and reducing drug degradation. Microspheres, nanoparticles and liposomes have been exploited [14].

Biodegradable polymers have been employed to fabricate microspheres to encapsulate L-DOPA. These systems provide prolonged release of the drug thanks to two simultaneous, slow processes: the diffusion of the drug through the pores of the microsphere and polymer degradation [15]. More recently, molecularly imprinted polymers (MIPs) have been proposed as a new drug delivery technology to achieve controlled and sustained release systems [16]. In contrast to polymer drug conjugates, where the drug is generally covalently bound to the polymer, drugs in MIPs are hosted through non-covalent interactions. MIPs based on cyclodextrins (CDs) have been reported in the literature [17]. The presence of CDs within an imprinted polymer network can improve the performance of the MIP [18]. Furthermore CDs can be used as pore templates to form nanoporous materials due to their peculiar structure and the ability to form inclusion complexes [19]. Indeed, they are cyclic oligosaccharides that exhibit a truncated cone shape structure with an interior hydrophobic cavity and a hydrophilic exterior site due to the presence of hydroxyl groups. Multiple approaches have been proposed to obtain MIPs based on CDs. For example, acryloyl-CD monomers can undergo radical polymerization to obtain the corresponding MIP. Condensation polymerization is less likely or limited to un-reactive template drugs [20].

Because of the large amount of reactive hydroxyl groups, CDs can act as polyfunctional monomers and be cross-linked using a wide variety of chemicals bearing two or more functionalities (e.g., dianhydrides, diisocyanates, epoxides, and dicarboxylic acids), producing insoluble, 3-dimensional polymers called “nanosponges” (NSs). The final properties of a CD-NS are strongly influenced by the nature of the cross-linker, the degree of cross-linking and the conditions of the synthesis reaction [21]. Several studies on the formulation and use of CD-NSs as nanocarriers have been conducted, showing that CD-NSs are a suitable delivery system for drugs, macromolecules and gases [22-29]. Shende et al. reported on the acute and repeated dose toxicity in animals of orally administered β-CD-NSs prepared using three types of cross-linker, i.e., pyromellitic dianhydride, 1,1’-carbonyldiimidazole and hexamethylene diisocyanate. In accordance with OECD guidelines 423 and 407, all formulations were proved to be safe at the tested concentrations of 2000 mg/kg and 300 mg/kg for acute and repeated dose toxicity, respectively [30]. Recently, molecularly imprinted NSs have been developed as biomimetic systems to evaluate blood glucose. The synthesis procedure used

pyromellitic dianhydride and glucose phosphate as the cross-linker and template molecule, respectively [31].

Based on NMR studies and predictive modelling previously reported in the literature [32, 33] for the ability of β-CD to form inclusion complexes with L-DOPA, β-CD was selected as the building block monomer for the preparation of a new L-DOPA delivery system. More specifically, in this work, polycarbonate β-CD-based NSs were obtained by cross-linking β-CD with 1,1'-carbonyldiimidazole. This reaction was conducted in the presence of highly reactive and unstable L-DOPA molecules to obtain a molecularly imprinted nanosponge (MIP-NS).

To the best of our knowledge, this is the first report of CD-NSs applied to the study of an oral formulation for the delivery of a drug for the treatment of a neurodegenerative disease.

MATERIALS AND METHODS

Materials

L-DOPA, 1,1'-carbonyldiimidazole (CDI), anhydrous N,N-dimethylformamide (DMF) and other reagents of analytical grade were purchased from Sigma-Aldrich (Saint Louis, MO, USA). β-cyclodextrin (β-CD) was a generous gift of Roquette Italia (Cassano Spinola-Italy) and was dried in oven at 120 °C to constant weight before use. DMF was dried immediately prior to use by the addition of CaH_2.

Synthesis of molecularly imprinted nanosponges

Molecularly imprinted nanosponges (MIP-NSs) were synthesized by reacting β-CD with different amounts of 1,1'-carbonyldiimidazole (CDI) in the presence of a variable amount of drug (2 % and 10 % with respect to the moles of βCD). A schematic representation of the preparation of a MIP-NS is depicted in Figure 1.

Briefly, to obtain MIP-NSs, anhydrous β-CD (mmoles are reported in Table 1) was dissolved, under vigorous stirring, in anhydrous N,N-dimethylformamide (DMF); then, L-DOPA was added. Finally, the required amount of CDI was introduced, and the reaction was allowed to react at 60 °C for 4 hours and at 90 °C for an additional 3 hours under a nitrogen atmosphere and protecting the reaction vessel from light by covering with aluminium foil. Four MIP-NSs were obtained by changing the amount of L-DOPA and the CDI/β-CD ratio, (Table 1. The numbers in brackets indicate the molar ratio between β-CD and the cross-linker).

When the reaction was completed, the monolithic block was crushed, treated with excess acetone and filtered under vacuum. The solid was extensively washed with acetone to remove DMF, imidazole

and possible unreacted monomers but not the drug (L-DOPA is almost insoluble in acetone). The L-DOPA-loaded NSs were then stored in hermetic vials that were protected from light.

For comparison, polycarbonate non-imprinted nanosponges (NIP-NSs) with two cross-linking degrees were synthesized in the same way but omitting L-DOPA. Successively, each type of NIP-NS in aqueous suspension (10 mg/mL) was loaded with L-DOPA. For this purpose, 6 mg of L-DOPA were added to 3 mL of each NIP-NS aqueous suspension and incubated at r.t. for 24 h under mild stirring. The loaded NIP-NSs (L-NIP-NSs) were recovered through centrifugation and were freeze-dried.

The re-loading properties of the MIP-NSs were evaluated by complete removal of L-DOPA via Soxhlet extraction in ethanol and water (50:50 v/v) and subsequent adsorption from an L-DOPA solution at room temperature for 24 hours. For comparison, a similar procedure was followed for the NIP-NSs.

L-DOPA quantitative determination

The quantitative determination of L-DOPA was performed by HPLC using a Perkin Elmer instrument (L2 Binary Pump, Perkin Elmer) with a UV-Vis spectrophotometer detector (LC 95, Perkin Elmer, USA) using an external standard method. A reverse-phase Hypersil ODS column (25 cm x 4.6 mm Varian, USA) was used with a mobile phase consisting of 980 mL of water, 16.5 g of sodium dihydrogen orthophosphate, 20 mL of methanol, 1 mL of 0.1 M EDTA and 1.2 mL of 0.5 mM sodium heptanesulphonate. The pH of the solution was adjusted to 3.4 with 1 M orthophosphoric acid. The analyses were performed at a flow rate of 0.9 mL/min at room temperature using a UV detector at 280 nm.

Nanosponge characterization

Fourier transform infrared (FTIR) spectra were recorded in the spectral range of 4000-650 cm^{-1} using a Perkin Elmer Spectrum 100 instrument in the attenuated total reflectance (ATR) mode with a diamond crystal using 32 scans per spectrum and a resolution of 4 cm^{-1}.

The surface morphology of the NIP-NSs and MIP-NSs was observed by field-emission scanning electron microscopy (FESEM, JEOL-JSM-6700F). The samples were examined after metallization with gold using the following experimental parameters: WD = 3.3 mm, EHT = 5.00 kV, and probe current = 130 pA.

Thermogravimetric analyses (TGA) were conducted on a TGA 2050 model from TA Instruments by heating samples contained in alumina pans at 10 °C/min from 40 to 700 °C in a nitrogen flow. Differential scanning calorimetry **(**DSC) was performed using a Perkin Elmer DSC/7 (Perkin Elmer,

CT, USA) equipped with a TAC 7/DX instrument controller. A heating rate of 10 °C/min was used in the 25–300 °C temperature range. Standard aluminium sample pans (Perkin Elmer) were used; an empty pan was used as the reference standard. Analyses were performed in triplicate on 5 mg samples under a nitrogen flow.

NMR studies

For NMR spectroscopy, one equivalent of β-CD was added to a sample containing 10 mM L-DOPA solution for the complexation study. For the kinetics study, three samples were prepared using 0.7 mL of a stock solution of L-DOPA (10 mM) in D_2O. One sample was used as the concentration reference; the two other samples contained empty MIP(1:8) (obtained from the sample MIP(1:8)+10%L-DOPA, after complete removal of L-DOPA) and NIP(1:8), with one equivalent of β-CD. At absorption equilibrium, which occurred within 24 hours of sample preparation, additional equivalents of polymer (up to five equivalents) were introduced. Quantitative ^1H spectra were recorded immediately after each addition of β-CD and for the following 24 hours. All samples were stored at room temperature away from light sources.

NMR measurements were performed on a spectrometer operating at 600 MHz for ^1H nuclei. The temperature was controlled to ±0.1 °C. For quantitative measurements, a 15 s pulse delay was selected. The 2D ROESY (rotating-frame Overhauser enhancement spectroscopy) experiments were performed using a mixing time of 0.3 or 0.6 s. The pulse delay was maintained at 5 s; 256 increments of 8 scans and 2K data points were collected for each spectrum. DOSY (diffusion ordered spectroscopy) experiments were conducted using a stimulated echo sequence with self-compensating gradient schemes, a spectral width of 6000 Hz and 64K data points. Typically, a value of 40 ms was used for Δ, 2 ms for δ, and g was varied in 20 steps (4 transients each) to obtain an approximately 90-95 % decrease in the resonance intensity at the largest gradient amplitude. The baselines of all arrayed spectra were corrected prior to processing the data. After data acquisition, each FID was apodized with 1.0 Hz line broadening and was then Fourier transformed. The data were processed with the DOSY macro (including the determination of the resonance heights of all signals above a pre-established threshold and the fitting of the decay curve for each resonance to a Gaussian function) to obtain pseudo two-dimensional spectra with NMR chemical shifts along one axis and calculated diffusion coefficients along the other. The gradient amplitudes in the DOSY experiments were calibrated using a standard sample of 99 % D_2O.

Determination of the size, polydispersity index and zeta potential of the nanosponges

The sizes and polydispersity indices of the two types of NSs were determined by dynamic light scattering using a 90 Plus particle sizer (Brookhaven Instruments Corporation, USA) equipped with MAS OPTION particle sizing software. The measurements were performed at a fixed scattering angle of 90° and at 25 °C. The samples were suitably diluted with filtered distilled water before each measurement. Zeta potential measurements were made using an additional electrode in the same instrument. For the zeta potential determination, the NS formulations were diluted with 0.1 mM KCl and placed in the electrophoretic cell, and an electric field of approximately 15 V/cm was applied.

L-DOPA stability studies

Stability studies on L-DOPA in solution were conducted spectrophotometrically. UV-Vis spectra were acquired with a Lambda 25 UV-Vis spectrophotometer (Perkin Elmer). Four solutions with different pH values, i.e., 2, 4, 7 and 9, were prepared by adding HCl or NaOH to ultrapure water; then, L-DOPA was introduced at a concentration of ~10^{-5} M. The spectra were collected between 200 and 800 nm after 10 minutes, 8 hours, 1, 2, 4, 8, and 16 days and were then overlaid. To evaluate the stability of the drug encapsulated in the NS, a freeze-dried sample was weighed, extracted and then centrifuged. After dilution of the supernatant, the solution was injected into the HPLC system for the quantitative determination.

Determination of the L-DOPA content in the nanosponges

A weighed amount (5 mg) of all types of L-DOPA-loaded NSs was dispersed in ultrapure water, sonicated for 30 min and then diluted with the HPLC mobile phase. After centrifugation, the supernatant was diluted and analysed by HPLC, as described before, to determine the drug concentration. The encapsulation efficiency and drug loading capacity were calculated using the following equations:

$$\text{Encapsulation efficiency} = \frac{\text{Actual amount of L-DOPA loaded in NSs}}{\text{Theoretical amount of drug loaded NSs}} \text{ x } 100$$

$$\text{Loading capacity} = \frac{\text{Actual amount of L-DOPA loaded in NSs}}{\text{L-DOPA loaded nanosponges weight}} \text{ x } 100$$

In vitro release study

The *in vitro* release studies of NS-encapsulated L-DOPA from MIP-NSs and NIP-NSs were conducted in phosphate buffer at pH 6.0 and pH 7.4 using multi-compartment rotating cells with a dialysis membrane (Sartorius, cut off: 12,000-14,000 Da). The donor phase consisted of an aqueous

NS suspension containing a fixed amount of L-DOPA. The receiving phase, which consisted of phosphate buffer at pH 6.0 or pH 7.4, was completely withdrawn and replaced with fresh medium at fixed time intervals. The experiment was performed in triplicate.
The concentration of L-DOPA released to the receiving phase was monitored for 48 hours using the HPLC method described above.

RESULTS AND DISCUSSION

Study of the stability of L-DOPA

Since the stability of L-DOPA is a critical issue for formulation studies, investigation of the chemical stability of L-DOPA to oxidation in aqueous solutions at different pH values was conducted by UV-Vis spectroscopy. The results are reported in Figure 2. In acidic solution (pH 2 and 4), all L-DOPA spectra were perfectly overlaid; no changes were observed over time. In the neutral solution, the initial degradation process became visible after 1 day. In basic solution (pH 9), 8 hours were sufficient to generate a detectable amount of oxidized L-DOPA. The characteristic absorption peak of L-DOPA appears at ~280 nm. The chemical species generated from the oxidation of L-DOPA [34] absorb all wavelengths from 200 to 800 nm, producing a dark brown solution. In particular, the main absorption peak of dopachrome is at ~475 nm.
The evidence of the low stability of L-DOPA in both alkaline and neutral environments, which was confirmed by the UV-Vis study, allowed us to better appreciate and note the protective effect of the NSs in aqueous media, as will be explained in the release study section.
The thermal stability of L-DOPA was investigated using thermogravimetric and infrared spectroscopic analyses. The TGA curve of L-DOPA is shown in Figure 3a. The weight of L-DOPA is constant up to 280 °C. Additionally, ATR-FTIR analyses of the drug before and after heat treatment similar to the one performed during the synthesis reaction (i.e., an isotherm at 60 °C for 4 hours, followed by a second isotherm at 90 °C for 3 hours in N_2) were performed. The two spectra are shown in Figure 3b, with perfect agreement between the two profiles. Therefore, according to TGA and ATR-FTIR analyses, L-DOPA is not affected by the thermal treatments used during the synthesis of MIP-NSs.
Previous experiments evaluated the chemical and thermal stability of L-DOPA, but the introduction of L-DOPA during the synthesis step is potentially detrimental to drug encapsulation in the polymer structure. Since L-DOPA carries a number of functional groups (i.e., -OH, -COOH, -NH_2) that can easily react with the cross-linker, modification of L-DOPA would be expected. Preliminary experiments confirmed that when CDI is added to a solution of L-DOPA in DMF, a cross-linked

insoluble polymer is obtained, even at room temperature (Figure 4a). Surprisingly, the HPLC analysis demonstrated that a negligible amount of L-DOPA (less than 0.5 wt %) was damaged during the polymerization reaction in the presence of β-CD. L-DOPA was extracted from the MIP-NSs and analysed by HPLC to determine the impact of the reaction at the molecular level. The interaction with MIP-NSs prevented the degradation of the drug. The chromatographic peak of the extracted L-DOPA showed the same retention time as that of the pure drug, which was used as a standard reference (Figure 4b). Moreover, no degradation products, which are easily detectable in the HPLC chromatograms of L-DOPA under stress conditions [34], were observed. In addition, the results are in agreement with the quantitative determination of the drug. Therefore, protective action of β-CD on L-DOPA during the synthesis reactions through the formation of inclusion complexes can be hypothesized.

To support this statement, DSC analyses were performed on MIP-NSs and showed the disappearance of the melting peak signal of L-DOPA at 310 °C. This behaviour can be ascribed to the molecular association of the drug with the NS structure (data not shown).

The affinity of L-DOPA for the CD cavity was investigated. Information about the complexing efficiency of β-CD in solution was obtained by analysing the translational diffusion coefficient D through DOSY experiments [35]. The diffusion coefficient is inversely proportional to the hydrodynamic radius (r_H), according to the Stokes-Einstein equation (Eq. 1):

$$D = kT/(6\pi\eta r_H) \quad (1)$$

where k is the Boltzmann constant, T is the absolute temperature, and η is the dynamic viscosity of the solution.

Since complexation leads to an increase in the apparent molecular size, variations in the diffusion coefficients are strictly related to aggregation phenomena. In fast exchange conditions, the observed diffusion coefficient for a given species (D_{obs}) is determined by the weighted average between the diffusion coefficient of the free molecule (D_f) and the diffusion coefficient of the molecule in the bound state (D_b), as shown in Eq. 2:

$$D_{obs} = x_f D_f + x_b D_b \quad (2)$$

where x_b and x_f are the molar fractions in the bound and free state, respectively.

When the molecular size of the host is significantly larger than the complexed substrate, D_b can be approximated by the translational diffusion coefficient of the complexing agent (D_C); hence, the

molar fraction of the complexed substrate in the bound state can be estimated using a single point determination (Eq. 3) [36], avoiding time-consuming titration experiments.

$$x_b = (D_{obs} - D_f)/(D_C - D_f) \quad (3)$$

For the chemical shift, there was no change in the proton frequency of the two molecules in the mixture sample compared with the pure compounds. Nevertheless, the variation in the diffusion coefficients indicate that inclusion complexation occurs (Table 2). A diffusion coefficient of 5.2 x 10^{-10} m^2s^{-1} was measured for pure L-DOPA, which only slightly decreased to 4.9 x 10^{-10} m^2s^{-1} in the presence of five equivalents of β-CD. Using the single point determination, we gave a rough estimate of the amount of L-DOPA complexed with β-CD, which was approximately 10 %.

The complexation stereochemistry was analysed by the ROESY experiment (Figure 5a); there were some dipolar correlations between protons H_5 and H_3 inside the cavity of β-CD and the aromatic protons of L-DOPA.

In particular, the H_5 and H_6 nuclei, which are located near the smaller opening of β-CD, interact with L-DOPA H_d and, in a minor way, with H_e. In contrast, the H_3 protons, which can be found near the larger opening of β-CD, have ROE effects with H_e and, to a slightly lesser extent, with H_c. No other intermolecular ROE correlations were found.

The recorded effects are consistent with the inclusion of the aromatic moiety of L-DOPA in the lipophilic cavity of the β-CD, as reported in Figure 5b, thus explaining the reduced reactivity of L-DOPA towards CDI and the preservation of its structure during polymerization.

Characterization of MIP-NSs

The presence of L-DOPA in the MIP-NSs structure was confirmed by ATR-FTIR analysis. In the infrared spectra of the four polycarbonate MIP-NSs (Figure 6), there is a characteristic peak due to the absorption of C=C in tri-substituted aromatic rings at ~1532 cm^{-1}. This peak does not appear in the IR spectra of the plain NSs used as reference. Because of the low concentrations of L-DOPA introduced during the synthesis step, any additional absorption peaks of L-DOPA are covered by the absorption bands of the NS.

The formulations containing the lowest amount of L-DOPA (2 %) were smaller (approximately 15 %) than those of MIPs containing 10 % L-DOPA (Table 3). The size difference might indicate a greater amount of L-DOPA associated with the polymer network. This behaviour is in agreement with the encapsulation efficiency results (Table 3). All MIP-NSs showed good ability to load L-

DOPA, with an encapsulation efficiency greater than 95 %. Moreover, the loading capacity of MIP-NSs is between 8 and 14 %. All the MIP-NSs showed greater encapsulation capacity than NIP-NSs. The lower zeta potential values of the MIP-NSs than those of the NIP-NSs is further experimental evidence of the different structural interaction (network) between the two polymer matrices and the effective interaction of the drug with the polymer matrices (Table 3).

The FESEM images shown in Figure 7 show no relevant differences in the morphology of the MIP and NIP-NSs.

The superior ability of empty MIP-NSs obtained from MIP-NSs after complete removal of L-DOPA to recognize and encapsulate L-DOPA in comparison with NIP-NSs was supported by NMR analysis. The quantitative NMR spectrum of the reference sample was recorded immediately after its preparation; quantitative spectra of the samples in the presence of the polymers were recorded within 24-72 hours after the addition of the polymers to ensure equilibrium and maximum absorption. Figure 8a shows the L-DOPA absorption percentage as a function of the amount of each type of NS. There is an almost linear correlation of the encapsulation extent for both polymers. The absorption of the substrate roughly doubles in the presence of the imprinted NS, with respect to the non-imprinted NS. By adding polymer containing 5 equivalents of β-CD, approximately 41 % of the L-DOPA was absorbed by the imprinted polymer, whereas barely 20 % was absorbed by the NIP, proving the effective molecular recognition of empty MIP-NSs towards L-DOPA.

L-DOPA in vitro release study from MIP-NSs

L-DOPA was released from all types of MIP-NSs with slow and biphasic kinetics over an extended period of time. Figure 8b shows the *in vitro* release profiles of encapsulated 10 % L-DOPA from MIP(1:4) and MIP(1:8). After 48 hours, they released 52.6 % and 56.8 % of the drug. Approximately 32 % of the drug was released by MIP(1:8)+10%L-DOPA after 6 hours, while only 26 % was released for the other type of MIP-NS (see the upper panel in Figure 8b), with no initial burst effects. The absence of an initial burst effect indicated that the drug is not adsorbed on the NS surface but strongly interacts with the NS structure. Pseudo zero-order kinetics were observed up to 4 h.

The modification of the crosslinker-CD ratio produced changes in the drug release patterns due to the different network structure. The MIP(1:4)+2%L-DOPA and MIP(1:8)+2%L-DOPA had slower release kinetics than the other two types of MIP-NSs. After 48 hours, MIP(1:4)+2%L-DOPA and MIP(1:8)+2%L-DOPA released only 30 % of the total amount of encapsulated drug (data not shown), while MIP(1:4)+10%L-DOPA and MIP(1:8)+10%L-DOPA released more than 50 %. This difference might be ascribed to the better fit of the L-DOPA molecule within the MIP-NS structure at low concentrations.

The release kinetics of L-DOPA from L-NIP-NSs were faster than from MIP-NSs, indicating a different type of association within the polymer nanostructures (data not shown).

Figure 8c shows the *in vitro* release profiles of MIP(1:4)+10%L-DOPA and NIP(1:4)+10%L-DOPA for comparison purposes. The L-DOPA release kinetics were faster from L-NIP-NSs than from the corresponding molecularly imprinted NSs. After 4 hours, MIP-NSs released approximately 21 % of the total amount of encapsulated drug, while L-NIP-NSs released approximately 77 %. No initial burst effects were observed for either formulation, indicating the good encapsulation of the drug. The inclusion of L-DOPA as a template during the synthesis favoured stronger interactions of the drug with the polymer structure and CD cavities, resulting in a slower and more prolonged release profile than L-NIP-NSs. The controlled and sustained kinetic behaviour might contribute to preventing critical oscillations in the L-DOPA plasma concentration.

CONCLUSIONS

New MIP-NSs for L-DOPA delivery were successfully synthesized using the drug as a template. Good encapsulation efficiencies and drug loading capacities were achieved. The protective effect of the NSs on L-DOPA molecules, which is due to the molecular interactions between L-DOPA and the polymer structure and the formation of inclusion complexes with the CD units, was highlighted during synthesis and storage. FTIR and thermal analyses confirmed the presence of the drug inside the NS structure after washing. Moreover, the NMR results showed that there is an inclusion of the aromatic moiety of L-DOPA in the cavity of the CD, which might be the reason for the effective performance of this molecularly imprinted drug delivery system. The *in vitro* studies indicated slow and controlled release kinetics over time, confirming that the MIPs have a strong ability to store the drug and sustain its release.

Based on these results, polycarbonate β-CD-based MIP-NSs are a promising new drug delivery system for the protection and prolonged release of L-DOPA for oral administration.

Acknowledgements

The authors thank Università di Torino research fund (ex-60%) for financial support and Prof. Silvia Bodoardo (Politecnico di Torino, Department of Applied Science and Technology) for the FESEM analysis.

REFERENCES

1. Clarke EG, Moffat AC. Clarke's Isolation and Identification of Drugs. London: The Pharmaceutical Press, 1986.
2. Hughes AJ, Daniel SE, Blankson S, et al. A clinicopathologic study of 100 cases of Parkinson's disease. Arc Neur 1993;50:140-148.
3. Puiu M, Babaligea I, Olmazu C, et al. Peroxidase-mediated oxidation of L-DOPA: A kinetic approach. Biochem Eng J 2010;52:248-254.
4. Eslami M, Zare HR, Namazian M, Thermodynamic Parameters of Electrochemical Oxidation of L-DOPA: Experimental and Theoretical Studies. J Phy Chem B 2012;116:12552-12557.
5. Zhou YZ, Alany RG, Chuang V, et al. Studies of the Rate Constant of L-DOPA Oxidation and Decarboxylation by HPLC. Chromatographia 2012;75(11-12):597-606.
6. Tahvanainen T, Haraguchi A. Effect of pH on phenol oxidase activity on decaying Sphagnum mosses. Eur J Soil Bio 2013;54:41-47.
7. Ngwuluka N, Pillay V, Du Toit LC, et al. Levodopa delivery systems: advancements in delivery of the gold standard. Exp Op Drug Del. 2010; 7(2):203-224.
8. Blacka KJ, Carlb JL, Hartleina JM, et al. Rapid intravenous loading of levodopa for human research: clinical results. J Neur Met 2003;127 (1):19-29.
9. Mouradian M. Should levodopa be infused into the duodenum?. Neurology 2005;64(2):182-183.

10. Lindner MD, Emerich DF. Therapeutic Potential of a Polymer-Encapsulated L-DOPA and Dopamine Producing Cell Line in Rodent Models of Parkinson's Disease. Cell Trans 1998;7(2):165-174.
11. Sudo J, Iwase H, Terui J, et al. Transdermal absorption of L-dopa from hydrogel in rats. Eur J Pharm Sci 1998;7(1):67-71.
12. Talukder R, Fassihi R. Gastroretentive delivery systems: a mini review. Drug Dev Ind Phar 2004;30(10):1019-1028.
13. Odak SP, Gidwani SK. Enhancement of aqueous solubility of levodopa by using 2-HP-B-cyclodextrin. Int J Pharm Sci 2011;3(1):933-938 (** a description of L-DOPA and cyclodextrin complexation).
14. Xiang Y, Wu Q, Liang L, et al. Chlorotoxin-modified stealth liposomes encapsulating levodopa for the targeting delivery against Parkinson's disease in the MPTP-induced mice model. J Drug Target 2012;20(1):67-75.
15. Arica B, Kaş H, Moghdam A, et al. Carbidopa/levodopa-loaded biodegradable microspheres: in vivo evaluation on experimental Parkinsonism in rats. J Control Rel 2005;102(3):689-697.
16. Alvarez-Lorenzo C., Concheiro A. Molecularly Imprinte Polymers for Drug Delivery. J Chrom B 2004;804:231-245 (** an important paper on drug delivery by molecular imprinted polymers).
17. Folch-Cano C, Yazdani-Pedram M, Olea-Azar C. Inclusion and Functionalization of Polymers with Cyclodextrins: Current Applications and Future Prospects. Molecules 2014;19:14066-14079.
18. Asman S, Mohamad S, Sarih NM. Influence of polymer morphology on the adsorption behaviors of molecularly imprinted polymer-methacrylic acid functionalized β-cyclodextrin. J Applied Polymer Sci, 2015;132(43):42720.
19. Kurkov SV, Loftsson T. Cyclodextrins. Int J Pharm 2013;453(1):167-180.
20. Asanuma H, Hishiya T, Komiyama M. Adv Mater 2000;12:1019-1030.

21. Trotta F. Cyclodextrin Nanosponges and their Applications. In Bilensoy E, editor. Cyclodextrins in Pharmaceutics, Cosmetics, and Biomedicine: Current and Future Industrial Applications. Hoboken, NJ: John Wiley & Sons, Inc., 2011 (** a wide overview on nanosponge applications).
22. Trotta F, Zanetti M, Cavalli R. Cyclodextrin nanosponges as drug carriers. Beilstein J Organic Chem 2012;8:2091-2099 (**a complete review on nanosponge characteristics).
23. Trotta F, Dianzani C, Caldera F, et al. The application of nanosponges to cancer drug delivery. Exp Op Drug Del 2014;11(6):931-941.
24. Seglie L, Martina K, Devecchi M, et al. The effects of 1-MCP on cyclodextrin based nanosponges to improve the vase life of Dianthus cariophyllus cut flowers. Postharvest Bio Tech 2011;59:200-205.
25. Daimay LV, Colthup NB, Fateley WG. The Handbook of Infrared and Raman Characteristic Frequencies of Organic Molecules. San Diego: Academic Press, 1991.
26. Cavalli R, Ansari AK, Bisazza A, et al. Nanosponge formulations as oxygen delivery systems. Int J Pharm 2010;402(1-2):254-257.
27. Swaminathan S, Vavia PR, Trotta F, et al. Nanosponges encapsulating dexamethasone for ocular delivery: formulation design, physicochemical characterization, safety and corneal permeability assessment. J Biomed Biotechnol 2013;9(6):998-1007.
28. Tejashiri G, Amrita B, Darshana J, Cyclodextrin based nanosponges for pharmaceutical uses: a review. Acta Pharm. 2013;63(3):335-358 .
29. Trotta F, Cavalli R, Swaminathan S, Cyclodextrin-based nanosponges: a versatile platform for cancer nanotherapeutics development WIREs Nanomed Nanobiotechnol 2016.
30. Shende P, Kulkarni YA, Gaud RS et al. Acute and Repeated Dose Toxicity Studies of Different β-Cyclodextrin-Based Nanosponge Formulations. J Pharm Sci. 2015;104:1856–1863.

31. Deshmukh K, Tanwar YS, Shende P, et al. Biomimetic estimation of glucose using non-molecular and molecular imprinted polymer nanosponges. Int J Pharm 2015;494(1):244-248.
32. Sompornpisut P, Deechalao N, Vongsvivut J. An Inclusion Complex of β-Cyclodextrin-L-Phenylalanine: 1H NMR and Molecular Docking Studies. ScienceAsia 2002;28:263-270.
33. Barros MCF, Ramos ML, Burrows HD, et al. Ternary mutual diffusion coefficients of aqueous [L-DOPA (1) + β-CD (2)] solutions at T = 298.15 K. J Chem Thermodynamics 2015;90:169-173.
34. Yong ZZ, Raid GA, Victor C, et al. Studies of the Rate Constant of L-DOPA Oxidation and Decarboxylation by HPLC. Chromatographia 2012;75(11):597-606.
35. Morris GA. Diffusion-ordered spectroscopy (DOSY). In Grant DM, Harris RK, editor. Encyclopedia of Nuclear Magnetic Resonance vol. 9. Chichester: John Wiley & Sons, Inc., 2002.
36. Cabrita EJ, Berger S. DOSY studies of hydrogen bond association: tetramethylsilane as a reference compound for diffusion studies. Magnetic Resonance in Chemistry 2001;39:S142-148.

CAPTIONS

Figure 1. Schematic representation of the synthesis of a MIP-NS.

Figure 2. UV-Vis spectra of L-DOPA solutions at 4 pH values: 2, 4, 7 and 9. The spectra collected after 10 minutes, 8 hours, 1, 2, 4, 8 and 16 days are overlaid in the 4 plots.

Figure 3. a) TGA of L-DOPA, programme used: equilibrium at 40°C, increase at 10°C/min to 700°C in N_2. b) ATR-FTIR analysis of L-DOPA (blue line) and L-DOPA after heating in TGA under a nitrogen flow at 60 °C for 4 hours and at 90 °C for an additional three hours (red line).

Figure 4. a) Cross-linked insoluble polymer obtained by reacting 1 g of L-DOPA with 1.644 g of CDI in 4 ml of anhydrous DMF at room temperature. The gelation point was reached after 1 day. b) HPLC analyses of L-DOPA. On the left: standard L-DOPA solution; on the right: L-DOPA extracted from MIP(1:4)+10% L-DOPA.

Figure 5. a) ROESY experiment results. b) Schematic representation of β-CD interaction with L-DOPA.

Figure 6. a) ATR-FTIR analysis of the L-DOPA-loaded NSs (red lines) compared with the plain NSs (blue lines). b) ATR-FTIR analysis of the L-DOPA free drug.

Figure 7. FESEM images of a) NIP(1:4) and b) MIP(1:4)+10%L-DOPA. Magnification 25 K.

Figure 8. a) L-DOPA adsorption percentage in empty MIP(1:8)+10%L-DOPA and NIP(1:8) NSs obtained by NMR. b) *In vitro* release profile of L-DOPA from the two types of MIP+10%L-DOPA NSs over time. c) *In vitro* release profile of L-DOPA from MIP(1:4) and L-NIP(1:4) NSs loaded with 10% L-DOPA.

Table 1. Qualitative and quantitative composition of reactants used in each NS synthesis. The numbers in brackets indicate the molar ratio of β-CD:cross-linker.

Table 2. Diffusion coefficients (D, $x10^{10}$ m^2s^{-1}) of β-CD and L-DOPA (5:1, [L-DOPA] = 10 mM) in the β-CD/L-DOPA mixture compared with pure compounds.

Table 3. Average size, polydispersity indices, zeta potential and encapsulation efficiency values of all types of MIP-NSs.

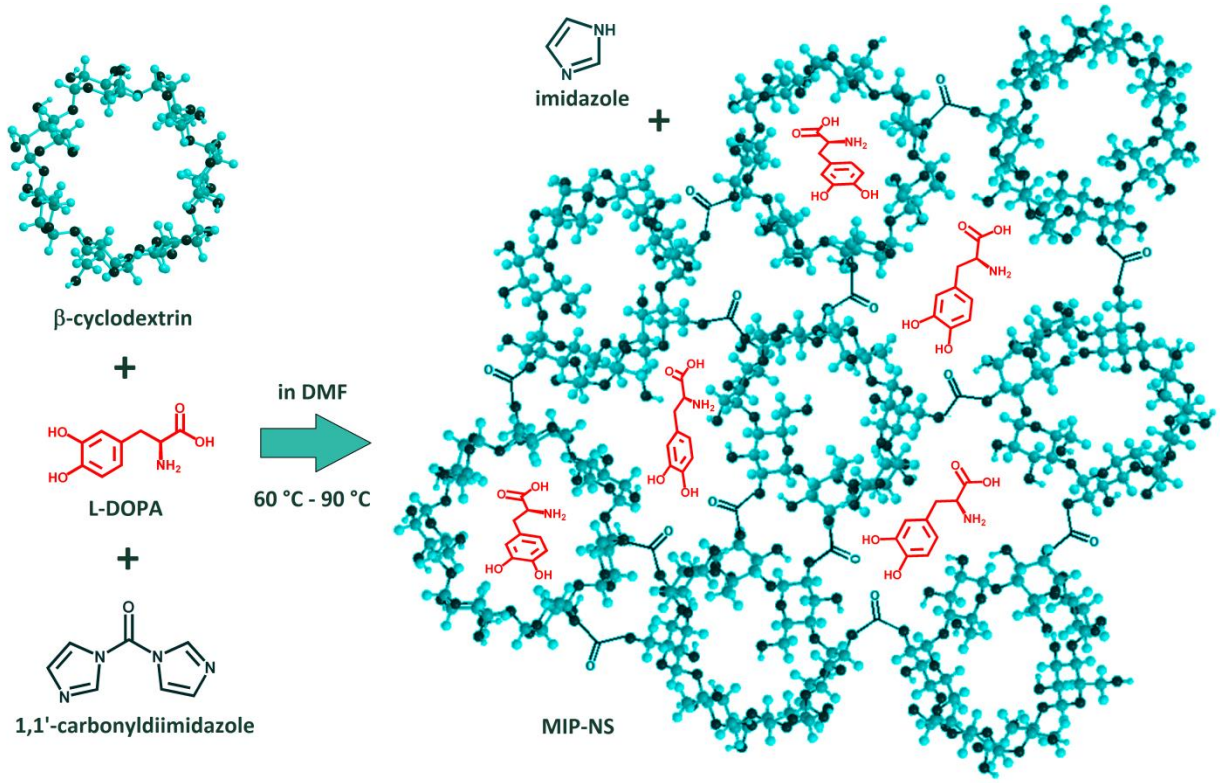
β-cyclodextrin
+
L-DOPA
+
1,1'-carbonyldiimidazole
in DMF
60 °C - 90 °C
imidazole
+
MIP-NS

FIGURE 1

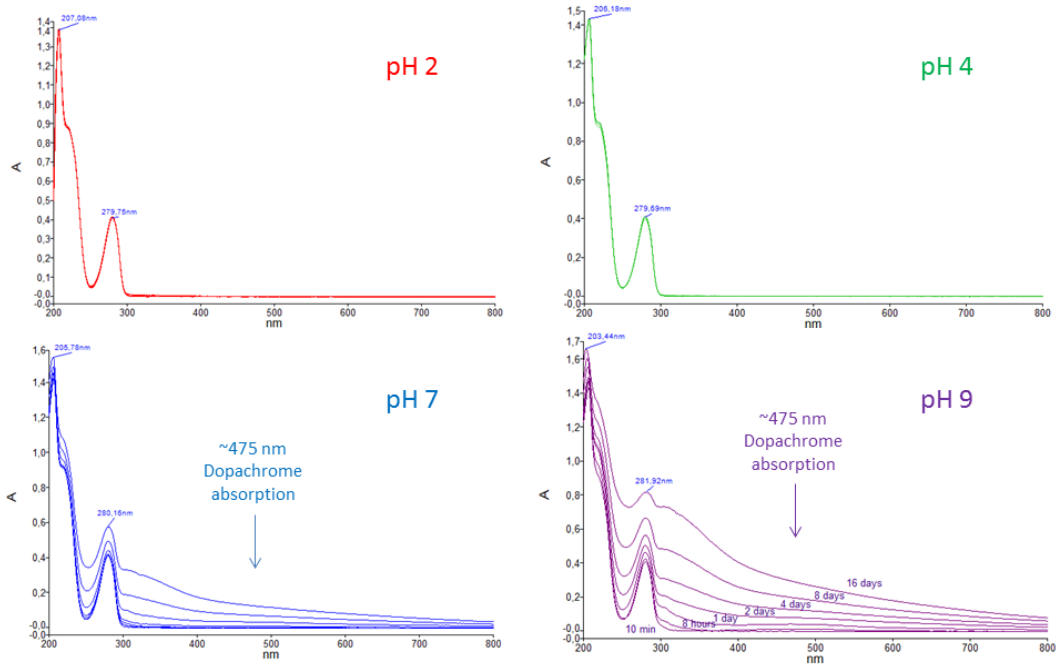
pH 2
207,08nm
279,76nm
pH 4
206,18nm
279,69nm
pH 7
205,78nm
280,16nm
~475 nm
Dopachrome
absorption
pH 9
203,44nm
281,92nm
~475 nm
Dopachrome
absorption
16 days
8 days
4 days
2 days
1 day
8 hours
10 min
A
nm

FIGURE 2

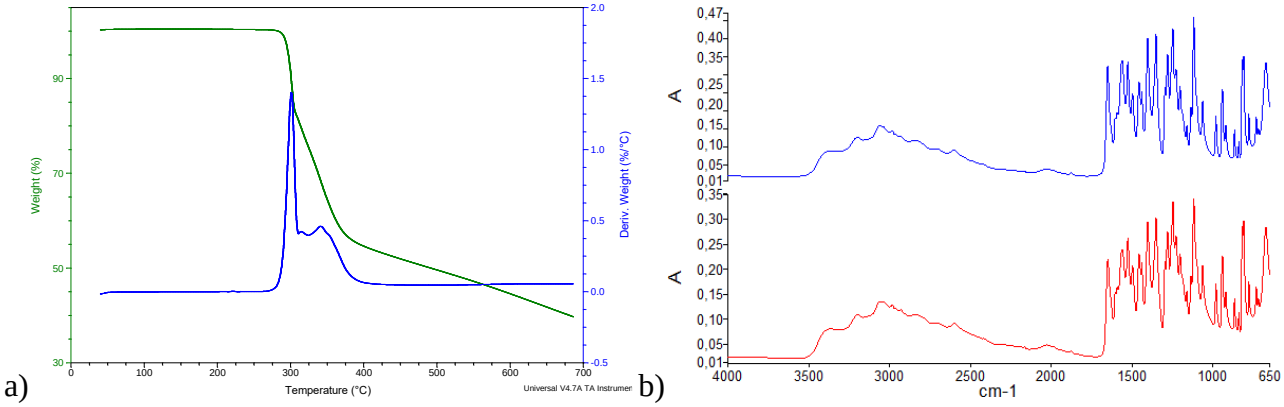
a)
Weight (%)
Deriv. Weight (%/°C)
Temperature (°C)
Universal V4.7A TA Instrumen
b)
A
A
cm-1

FIGURE 3

a)  b) 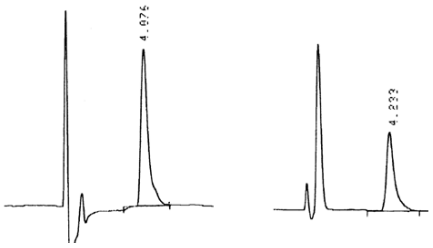

FIGURE 4

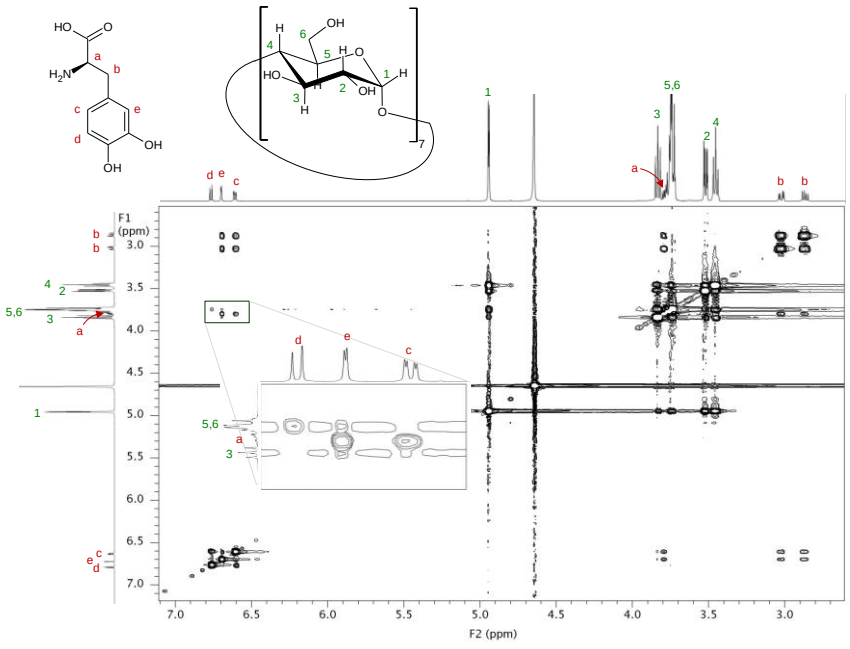
F1 (ppm)
F2 (ppm)
3.0
3.5
4.0
4.5
5.0
5.5
6.0
6.5
7.0
7.0
6.5
6.0
5.5
5.0
4.5
4.0
3.5
3.0

a)

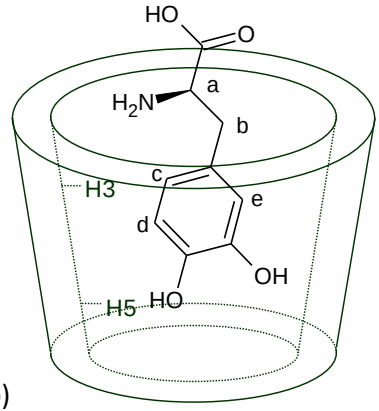
HO
O
H2N
a
b
c
H3
d
e
OH
H5
HO

b)

FIGURE 5

a)

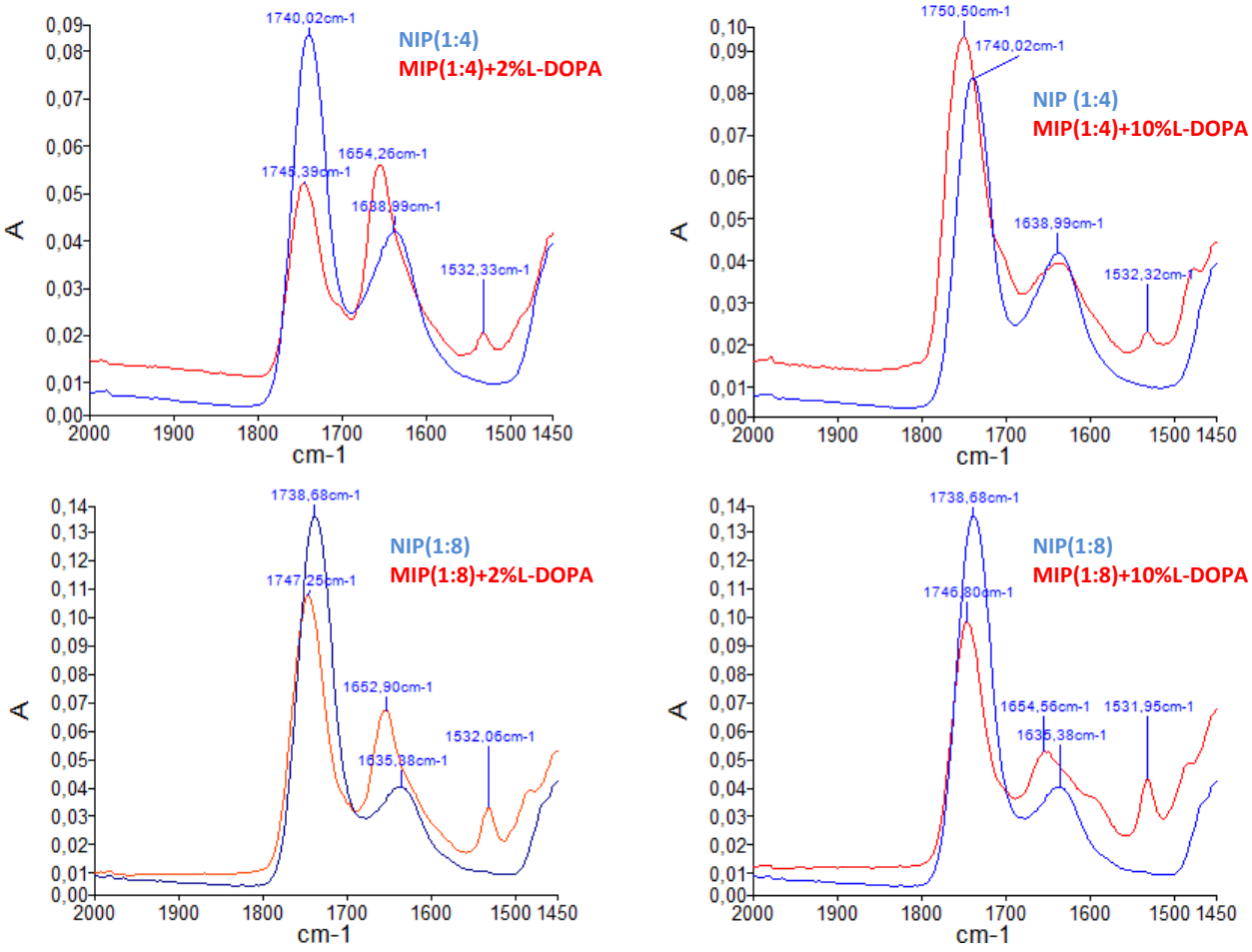
1740,02cm-1
NIP(1:4)
MIP(1:4)+2%L-DOPA
1654,26cm-1
1745,39cm-1
1638,99cm-1
1532,33cm-1
A
cm-1
1750,50cm-1
1740,02cm-1
NIP (1:4)
MIP(1:4)+10%L-DOPA
1638,99cm-1
1532,32cm-1
1738,68cm-1
NIP(1:8)
MIP(1:8)+2%L-DOPA
1747,25cm-1
1652,90cm-1
1532,06cm-1
1635,38cm-1
1738,68cm-1
NIP(1:8)
MIP(1:8)+10%L-DOPA
1746,80cm-1
1654,56cm-1
1531,95cm-1
1635,38cm-1

b)

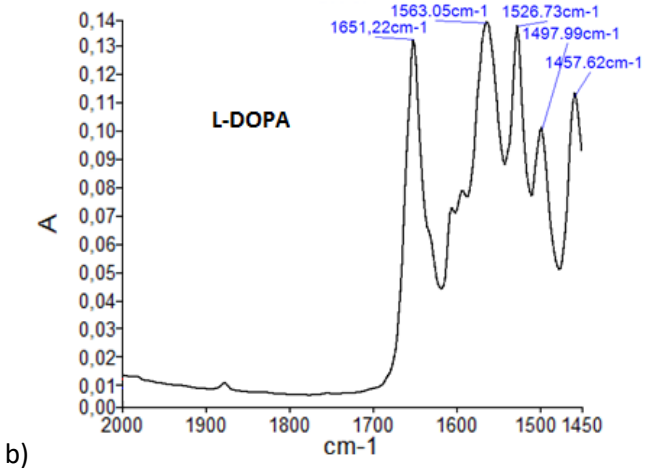
1563.05cm-1
1526.73cm-1
1651,22cm-1
1497.99cm-1
1457.62cm-1
L-DOPA
A
cm-1

FIGURE 6

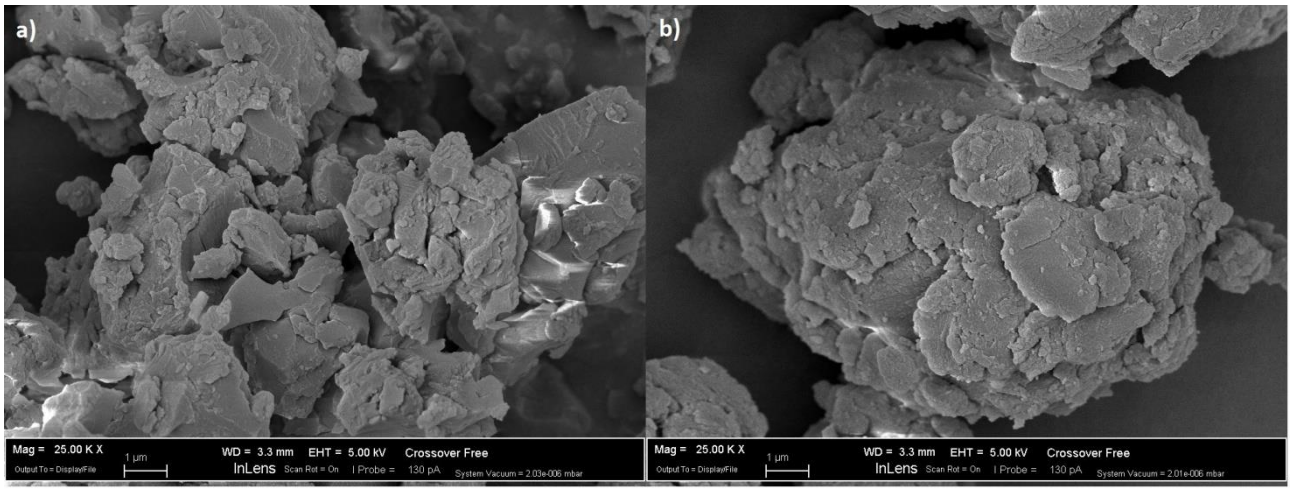
a)
Mag = 25.00 K X
1 µm
WD = 3.3 mm EHT = 5.00 kV Crossover Free
Output To = DisplayFile
InLens Scan Rot = On I Probe = 130 pA System Vacuum = 2.03e-006 mbar
b)
Mag = 25.00 K X
1 µm
WD = 3.3 mm EHT = 5.00 kV Crossover Free
Output To = DisplayFile
InLens Scan Rot = On I Probe = 130 pA System Vacuum = 2.01e-006 mbar

FIGURE 7

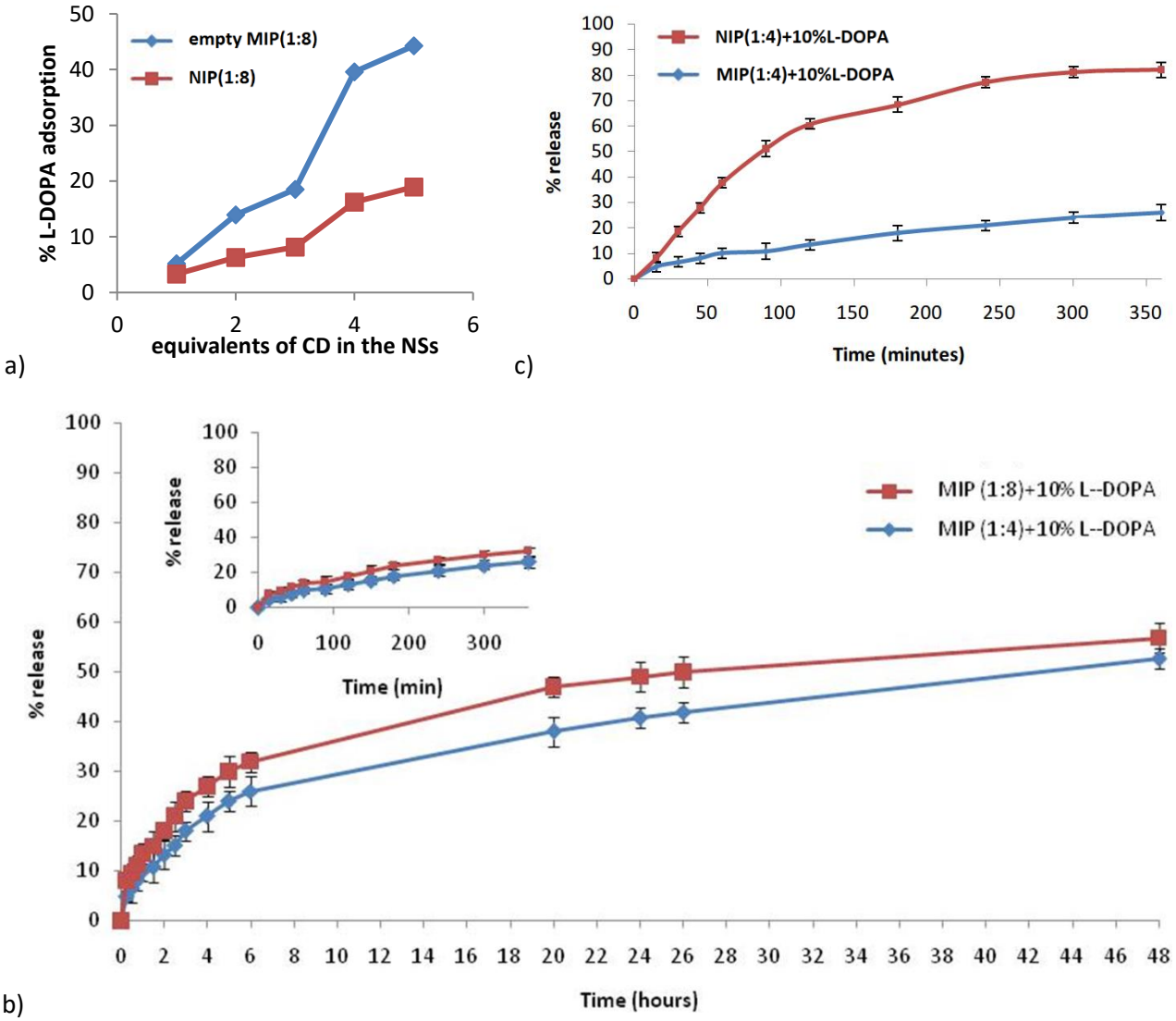
a)
% L-DOPA adsorption
empty MIP(1:8)
NIP(1:8)
equivalents of CD in the NSs
c)
% release
NIP(1:4)+10%L-DOPA
MIP(1:4)+10%L-DOPA
Time (minutes)
b)
% release
Time (min)
MIP (1:8)+10% L--DOPA
MIP (1:4)+10% L--DOPA
Time (hours)

FIGURE 8

Nanosponge Samples	DMF (ml)	β-CD (mmol)	L-DOPA (mmol)	CDI (mmol)
NIP(1:4)	60	8.81	-	35.24
NIP(1:8)	60	8.81	-	70.48
MIP(1:4)+2%L-DOPA	60	8.81	0.18	35.24
MIP(1:8)+2%L-DOPA	60	8.81	0.18	70.48
MIP(1:4)+10%L-DOPA	60	8.81	0.88	35.24
MIP(1:8)+10%L-DOPA	60	8.81	0.88	70.48

TABLE 1

Sample	**$D_{\beta\text{-CD}}$**	**$D_{\text{L-DOPA}}$**
β-CD	3.0	-
L-DOPA	-	5.2
β-CD/L-DOPA	2.7	4.9

TABLE 2

Nanosponge Sample	Average size (nm)	Polydispersity index	Z-Potential (mV)	Encapsulation Efficiency (%)
MIP(1:4)+2%L-DOPA	346.3 ± 6.4	0.207 ± 0.021	-12.26 ± 1.27	95.2
MIP(1:8)+2%L-DOPA	374.7 ± 8.2	0.215 ± 0.018	-11.4 ± 1.32	95.6
MIP(1:4)+10%L-DOPA	411.6 ± 7.7	0.221 ± 0.015	-14.20 ± 1.03	97.8
MIP(1:8)+10%L-DOPA	421.2 ± 9.3	0.203 ± 0.013	-22.3 ± 1.05	98.2
NIP(1:4)	356.5 ± 5.3	0.204 ± 0.022	-25.74 ± 0.36	90.5
NIP(1:8)	381.7 ± 10.6	0.214 ± 0.014	-26.21 ± 1.09	82.1

TABLE 3